Temporal Information Processing with an Integrated Laser Neuron

Hsuan-Tung Peng* Student Member, IEEE, Gerasimos Angelatos, Thomas Ferreira de Lima Student Member, IEEE, Mitchell A. Nahmias, Alexander N. Tait, Siamak Abbaslou, Bhavin J. Shastri, Member, IEEE Paul R. Prucnal, Life Fellow, IEEE

Abstract—Spiking neural networks enable efficient information processing in real-time. Excitable lasers can exhibit ultrafast spiking dynamics, and when preceded by a photodetector in an O/E/O link, can process optical spikes at different wavelengths and thus be interconnected in large neural networks. Here, we experimentally demonstrate and numerically simulate the spiking dynamics of a laser neuron fabricated in a photonic integrated circuit. Our spiking laser neuron is shown to perform coincidence detection with nanosecond time resolution, and we observe refractory periods in the order of $0.1\,\mathrm{ns}$. We propose a method to implement XOR classification using our laser neurons, and simulations of the resultant dynamics indicate robust tolerance to timing jitter.

Index Terms—Neuromorphic photonics, photonic integrated circuits, photonic neural networks, excitable lasers, spiking neural networks.

I. INTRODUCTION

Spike processing is a sparse coding scheme using distributed and asynchronous pulses to process information both spatially and temporally. Compared to conventional von Neumann architecture, this spiking paradigm offers dramatic increases in power efficiency [1] and processing ability in certain domains such as learning, optimization and pattern recognition [2]-[4]. In addition to power and computing efficiency, it has been established that the temporal dynamics of spiking plays an important role in neuronal information processing [5]–[7]. Through threshold response to signals and by using temporal correlation to process information, spiking dynamics enables a computing paradigm that combines the noise robustness of digital communication with the bandwidth efficiency of analog processing. This revolutionary potential has sparked a bloom in the development of spiking hardware across various physical platforms [8]-[20]. Due to low cross-talk in interconnects and ultrafast laser dynamics, integrated photonics are particularly well-suited to implement neuromorphic systems that processes signals at very high speed and bandwidth [21]-[25]. The fundamental unit of a spike processor is the neuron, whose essential dynamical properties of temporal integration, threshold response, and

*Corresponding author: hpeng@princeton.edu

B.J.S. is also with the Department of Physics, Engineering Physics & Astronomy, Queen's University, Kingston, ON KL7 3N6, Canada.

Manuscript received XX XX, XXX; revised XX XX, XXX.

refractory period must be well-understood.

The refractory period is the time interval following a neuron's spike wherein the system cannot be excited again. It is a fundamental component of excitability [26], [27], during which the neuron returns to its rest state, thus enabling repeatable spiking. The existence of a refractory period also sets the maximal spike firing rate, an necessary property for spike processing using rate coding [28]. Temporal integration refers to the capacity of a neuron to integrate different presynaptic stimuli in time, and threshold response the neuron's ability to produce a sharp robust spike once this integrated stimulus exceeds the excitability threshold. This ability to integrate a signal and compare against a threshold enables a neuron to perform coincidence detection: the neuron's threshold can be set such that individual input pulses do not produce a response, but if two (or more) arrive within some temporal window their integrated sum exceeds the excitability threshold, generating a spike. Coincidence detection is the fundamental process in various spatial-temporal recognition tasks [10], [29]–[33]. In this work, we proposed an integrated photonic circuit spiking processor, and studied its temporal dynamics both experimentally and theoretically. A method to implement XOR classification is also proposed to demonstrate the potential of this spiking platform to perform computation. The paper is organized as follows: The device architecture, experimental setup and methods are described in Section II. In Section III we experimentally and theoretically study the fundamental dynamical features of this device: the threshold response to increasing integrated inputs, the refractory period following stimulus, and the ability to perform coincidence detection. Finally, in Section IV we simulate XOR classification using our laser neurons in the presence of timing jitter.

II. A PHOTONIC SPIKE PROCESSOR

The proposed photonic spike processor is shown in Fig. 1(b); it consists of a two-section distributed feedback laser (DFB) and a pair of high-speed balanced photodetectors (BPDs), the former generates spikes and the latter acts as the summation unit in a neural network. In this architecture, BPDs receive optical spikes and drive the adjacent DFB laser, which performs spiking dynamics and converts the signal back to the optical domain. This concept of direct analog O/E/O (optical to electrical to optical) link is first introduced in Ref. [34], and has been applied to excitable lasers showing the capability of

H.-T.P., G.A., T.F.L., M.A.N., A.N.T., S.A., B.J.S. and P.R.P. are with the Department of Electrical Engineering, Princeton University, Princeton, NJ 08544, USA.

A.N.T. is also with National Institute of Standards and Technology, Boulder, Colorado 80305, USA

integrated laser neurons to process many distinguishable, high bandwidth input signals simultaneously [23]. This represents a viable direction towards scalable photonic spiking neural networks.

In Ref. [21], we have shown preliminary spike generation results for this device. In this work, we focus on the temporal dynamics of the integrated spiking laser neuron, and its application to solve an XOR problem.

A. Device

Nine laser neurons on an integrated photonic chip are shown in Fig. 1(a). The basic composite structures of the laser neuron are a two-section DFB laser, high-speed BPDs, and lithographically-defined metal wires connecting detectors and the lasers together. The proposed two-section DFB laser is composed of a small section with length $75.0 \,\mu\mathrm{m}$, and a large section with length $125.0 \,\mu\mathrm{m}$. The two sections are optically coupled but electrically separated by $75.0 \,\mu\mathrm{m}$ such that independent electrical sources can be provided to each section. A current I_L flowing into the large section provides gain to the laser cavity, and the current I_S to a smaller section adjusts internal cavity absorption level. The interaction between the two sections allows for the excitable behavior exhibited by the device. [21] The balanced photodetectors PD1 and PD2 are connected only to the large section, as seen in Fig. 1. The photocurrent generated by PD2 will flow into large section as an excitatory perturbation, while PD1 acts as inhibitory synapse because its photocurrent flows out of the large section. All the components can be found in the standard process design kits (PDKs) [35] which allows scalable laser neural networks. The chip was fabricated by the Heinrich Hertz Institute through JePPIX consortium in a standard, indium phosphide PIC platform. The details of the architecture of the chip and the device parameters can be found in Ref. [21].

B. Experimental Setup

To investigate temporal dynamics of the spiking laser neuron, we programmed optical pulses and sent them to the bottom photodetector (PD2 in Fig. 1(b)) to provide excitatory stimulus to the system. The input optical pulses were generated by modulating a continuous-wave DFB laser source (ILX Lightwave 7900B) with a high speed Mach-Zehnder modulator (JDSU OC-192). The modulation signals were programmed by a high speed pulse patter generator (PPG, Anritsu MP 1763B), and a sampling scope (Tektronix DSA8300) were used to measure both input and output optical signals. To compensate the loss (≈ 20 dB) between spot-size converters and v-groove fiber array, we used high power EDFAs (PriTel FA-30) to amplify optical input and output pulses, and tunable bandpass filters (Santec OTF-320) were connected to the output of EDFAs for noise filtering. For different experiments, the input pulses were programmed differently and detailed in the Section. II-C.

For the laser system, the electrical controls of laser are on the edge of the chip. In Fig.1(b), the left metal pads were connected to DC probes (GGB MCW-27-3050-A), and the

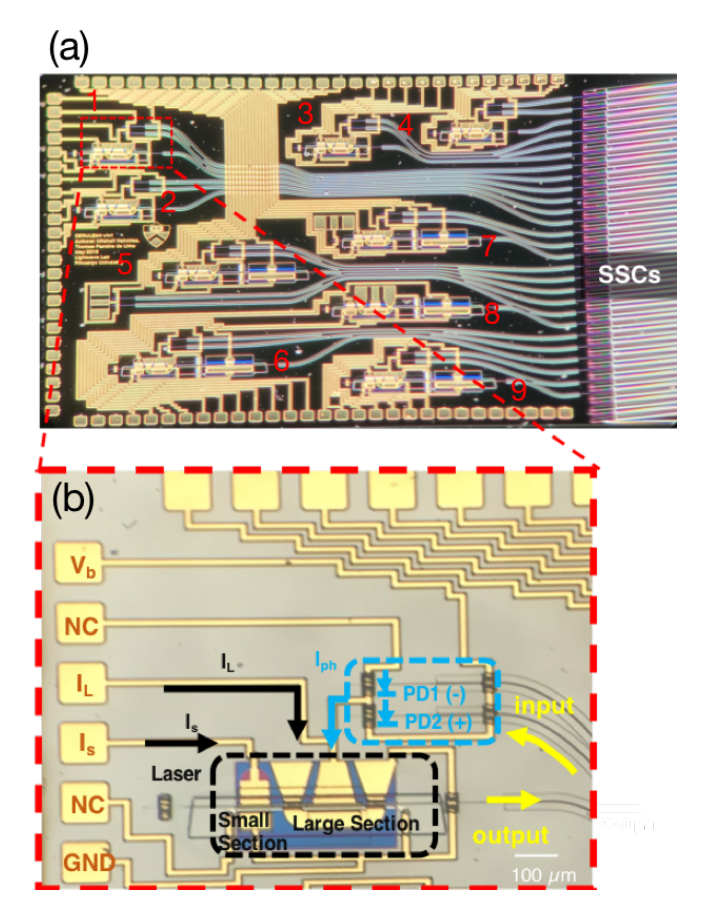


Figure 1. (a) A set of nine photonic laser neurons on an InP-based integrated photonic chip. A photonic spiking neuron used in the experiment is highlighted in red. On the right of the chip are the spot size converters (SSCs), which are aligned with a V-groove fiber array providing coupling of optical signals to on-chip waveguides. (b) The micrograph of a photonic laser neuron. A two-section DFB laser and a pair of balanced photodetectors are highlighted in black and blue respectively. The metal pads shown on the left are used to source current to two-section DFB laser and control the bias of photodetectors. GND: Ground, I_L : Current to large section of laser, I_S : Current to small section, V_b : Voltage bias to PD2, NC: Not Connected to any electrical source in this work. Adapted with permission from Peng *et al.*, *IEEE Journal of Selected Topics in Quantum Electronics* 24 6 (2018) Ref. [21].

current and voltage sources are provided by three source meters (Keithley 2400). In this work, only the excitatory photodetector (PD2) was used. The reverse bias V_{PD2} of PD2 was provided by V_b . ($V_{PD2} = V_b - V_L$, where V_L is the voltage of large section.) The input optical signals were sent to PD2 through on-chip waveguide, which generates the photocurrent I_{ph} that forms the excitatory perturbation to the large section of DFB laser. This setup is shown in Fig. 2.

C. Method

Our goal is to demonstrate ultrafast laser temporal dynamics, thereby emulating a leaky integrate-and-fire (LIF) neuron model [20], [27]. We designed three sets of experiments to show the temporal properties of the integrated laser neurons, investigating pulse width response, refractory dynamics, and coincidence detection. All the laser neurons are designed to be identical, and here the refractory dynamics is demonstrated on

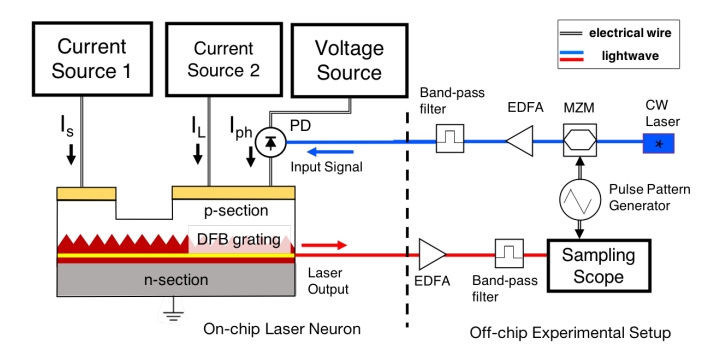


Figure 2. Schematic figure of the experimental setup, with input and output optical signals highlighted in blue and red. Current sources 1 and 2 are used for the biases of small section and large section of DFB laser respectively. The voltage source controls the reverse bias of the excitatory PD (PD2).

 1^{st} neuron, and the pulse width and coincidence experiments are implemented on 4^{th} neuron, as labeled in Fig. 1 (a). The resultant findings are reinforced via numerical simulation of the two-section laser dynamics with the Yamada model [36], [37]. In all experiments, the time-dependent traces of input and output powers on the chip were first measured by the sampling scope, and then converted to powers by matching the time average of each signal to the average optical power. The input (output) average optical power was calculated by subtracting (adding) the measured off-chip power with the expected SSC-fiber interface loss. The input pulses and settings used in each set of experiments are summarized below:

- 1) Pulse Response: We used a PPG to generate a pattern that consisted of two input pulses separated by 50 ns: The sum of widths of two pulses was set to be $2.4 \,\mathrm{ns}$, with the width of the first pulse ranging from $0.1\text{-}1.2\mathrm{ns}$. This setting is to ensure the average power is constant for all measurements so that all the input signals measured by the sampling scope can be converted to power using the same factor. In this experiment, we used the 4^{th} laser neuron labeled in Fig. 1(a) and biased it close to the lasing threshold. The bias conditions are given as follows: $I_L = 10.6 \,\mathrm{mA}$, $I_S = 0.0 \,\mathrm{mA}$, $V_{PD2} = 3.67 \,\mathrm{V}$.
- 2) Refractory Period: To analyze the refractory dynamics of our system, we generated two identical input pulses, each of which has energy $10.4\,\mathrm{pJ}$, sufficient to excite a spike output. The pulses are input to the excitatory photodetector with a center-to-center temporal separation varying from $0.2\text{-}2.2\,\mathrm{ns}$. The 1^{st} laser neuron (labeled in Fig. 1(a)) was used, and it was again biased close to lasing threshold under the conditions: I_L = $6.2\,\mathrm{mA}$, $I_S = 0.0\,\mathrm{mA}$, $V_{PD2} = 3.75\,\mathrm{V}$.
- 3) Coincidence Detection: In this experiment, we generated two input pulses, each of which individually does not have enough energy to excite a spike, and programmed the temporal center-to-center distance of two input pulses from 0.4-5.4 ns. The same neuron and bias condition as for the pulse response experiment was used.
- 4) Numerical Simulation: We simulate the dynamics of the laser neuron in response to injected current pulses using the well-studied Yamada model [20], [36], [37], which describes

a single-mode laser with two independent carrier sections:

$$\dot{I} = \kappa (G - Q - 1) I + \beta_n$$

$$\dot{G} = \gamma (A + \theta i_{in}(t) - (1 + I) G)$$

$$\dot{Q} = \gamma (B - (1 + aI) Q)$$
(1)

In the above, I is the laser intensity, while G and Q are scaled carrier densities in the two sections, with the former describing gain and the latter describing saturable absorption, all of which are dimensionless. κ and γ are the photon and carrier relaxation rates, which we here assumed to be the same in both sections. A and B are the biases to each section, and a is the differential absorption relative to the gain. θ connects the injected current from the photodetectors $i_{\rm in}(t)$ to the resultant gain, and $\beta_n \ll \kappa, \gamma$ is the contribution to the intensity from spontaneous emission and other noise sources. The parameters in Eq. (1) are calculated in terms of fundamental device constants via analogy to the rate equations [20], which we obtain by fitting simulations to data for each of the experiments described above.

III. RESULTS AND ANALYSIS

A. Theoretical Model

The Yamada model exhibits class I excitability due to the presence of a saddle-node bifurcation. Such systems are characterized by the onset of self-oscillations (repeated spiking) at zero frequency under constant stimulus above threshold. Measurements and simulations indicate that for the present device, this bifurcation occurs for I < 0 and is thus outside the physical phase-space, a consequence of the estimated $a \simeq 1$. As a result, this laser neuron does not undergo a self-oscillation transition under increased DC bias and instead possesses a nonlinear ReLU-like (rectifier) activation function. Although not a true "class I excitable system", the physical (I > 0)phase portrait still exhibits strong signatures of this nearby bifurcation, such that perturbations in G exceeding a threshold result in large excursion in phase space before refracting. To be more specific, the laser neuron is operated in a regime with a single stable fixed point at low $I = I_0$ (populated via noise β_n). Under small perturbations in G, the system quickly returns to this steady state. However, as a consequence of this nearby saddle-node bifurcation, the phase portrait is such that inputs sufficiently large to displace to G - Q > 1 result in a trajectory which rapidly spikes to $\{I \gg I_0, G \to 0, Q \to 0\}$. The laser becomes effectively inverted and the intensity grows exponentially. Since we have $\kappa \gg \gamma$, the spike is short and sharp; G and Q then recover towards their steady states (A and B) more slowly. This results in the refractory period seen in Fig. 4: the gain remains depleted after the initial spike, which suppresses successive excitation. This response depends critically on the presence of β_n : for $\beta_n = 0$, I = 0 is an invariant plane and no perturbation in G will produce a spike. Further, since $I_0 \propto \beta_n$, this noise significantly influences the sensitivity to inputs above threshold and the threshold itself. The laser neuron thus is able to temporally integrate input currents, spike once this exceeds a threshold, and exhibits a refractory period. These features, demonstrated in the results below, reinforce the inherent excitability of this system and its utility in spike processing.

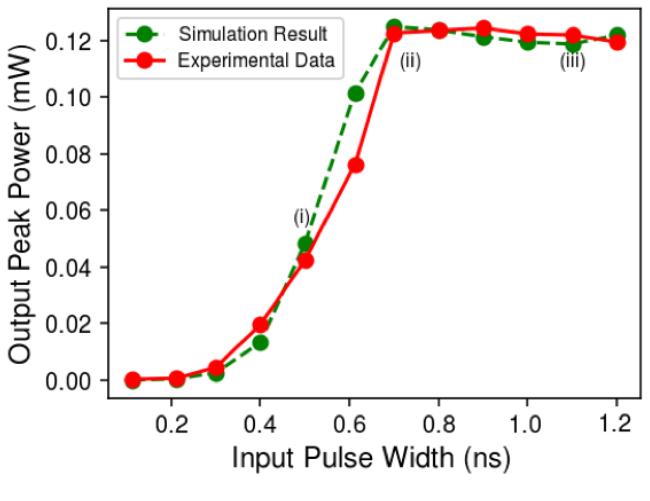
B. Pulse Response

To demonstrate the threshold optical-to-optical response in our photodetector-laser system, we measured the output pulse in response to pulses of increasing input energy, achieved by varying the pulse width as described in Sec. II-C1. As shown in Fig. 3, the laser neuron has a strongly nonlinear response to increasing pulse width. The peak power of the output spike grows exponentially with input pulse width and then suddenly saturates at $0.7 \, \mathrm{ns}$. The peak output spike power is constant with input pulse width beyond this threshold at 0.7 ns. The output waveform profile shows that the system has short-term memory, such that the perturbation within a certain temporal range can contribute to build up the output peak power. Increasing the input pulse length beyond this point results in a wider spike output with the same peak power. The output power is about 2 orders of magnitude smaller than the input, largely due to poor coupling efficiency.

These features and the observed response dynamics are reproduced well via simulations of Eq. (1), with parameters a=1, $\gamma=8\,\mathrm{GHz},~\kappa=65\,\mathrm{GHz},~A-B=0.70,~\theta=0.072\,\mathrm{mA}^{-1},~\beta_n=2.5\,\mathrm{MHz}.$ As described in Sec. III-A, short pulses do not displace the system sufficiently from the steady state to generate a spike. As the pulse energy increases towards the threshold, the peak output pulse power grows exponentially as the response phase space trajectory gets closer to the spiking trajectory. Once sufficient energy arrives at the laser neuron (0.7 ns of input pulse), the system is able to complete a spike and additional input current beyond this has little influence on the resultant trajectory, yielding the plateau in peak output power seen.

C. Refractory Period

As suggested in Sec. III-A, the laser neuron processes a refractory period due to the slower recovery of carriers to their steady-state density following a pulse. If a second input pulse arrives within this refractory period, the spike response is suppressed. To study this feature, we investigated the response of the spiking laser neuron to a pair of identical input pulses with varying separation in Fig. 4. One can make a distinction between absolute and relative refractory period. Within the absolute refractory period, the laser neuron cannot be excited and no second spike is seen, as shown in inset (i) of Fig. 4 (input temporal separation $0.3 \,\mathrm{ns}$). In the relative refractory period, excitation is possible, although the amplitude of the second is reduced compared to the initial spike. When the temporal separation of two input pulses is large enough (greater than 0.5 ns), the neuron will fire two spikes with identical peak power as the inset (iii) of Fig. 4 shows. Within the relative refractory period, the difference between first and second peak power is seen to decrease exponentially as the temporal separation of input pulses increases. The absence of a second pulse for input separations up to 0.3 ns indicates that this is the approximate absolute refractory period, while the relative refractory period is $\sim 0.5 \,\mathrm{ns}$, since for separations



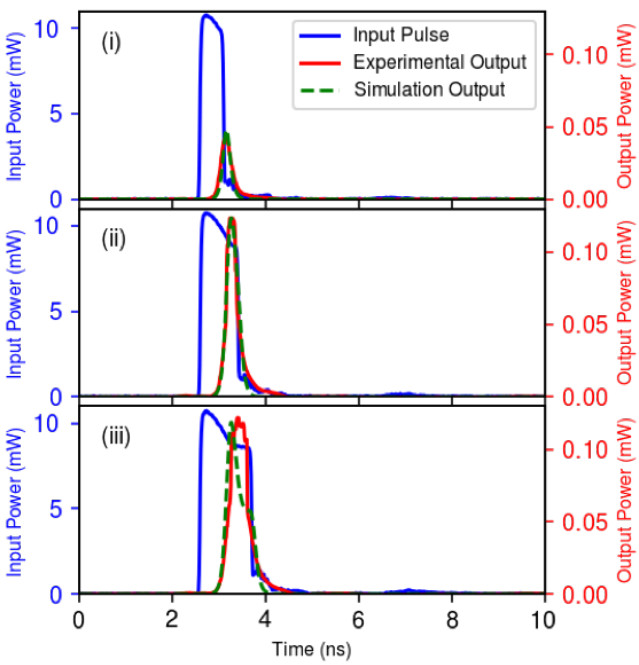


Figure 3. Simulated (green) and measured (red) laser neuron output in response to input pulses of increasing width. Dynamics are shown for widths of $0.5\,\mathrm{ns}$, $0.7\,\mathrm{ns}$, and $1.1\,\mathrm{ns}$ in (i), (ii), and (iii) respectively, with the input signal in blue and the simulated and measured output pulses in dashed green and red.

greater than this the two output spikes are identical. The observed refractory period results in a maximal firing rate of 2 GHz for the spiking laser neuron. It is worth noting that our system behaves similarly to and has the same order of refractory period as the device in [9], despite having a different photonic neuron architecture and excitation method.

Simulation of the Yamada model again emulates these experimental observations well, with A-B=0.66, $\theta=0.10\,\mathrm{mA}^{-1}$, $\beta_n=44\,\mathrm{MHz}$, and other parameters unchanged. Recall that a different laser neuron, with different bias conditions, is used in this experiment. As noted earlier, the refractory period originates from the slow relative recovery of carrier inversion densities G and Q, which are forced to 0 during a

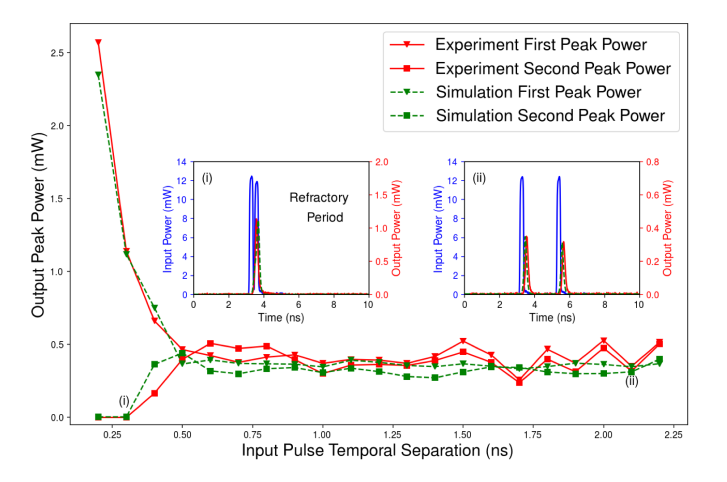


Figure 4. Response to successive input pulses as a function of their separation, demonstrating the laser neuron's refractory period. The peak amplitude of the response to each input pulse as observed experimentally and simulated are shown in red and green respectively. The triangles represent the peak power of the first output spike, and the squares represent the peak power of the second output. In addition, input and output signal traces are shown for separations 0.3 ns and 2.1 ns in insets (i) and (ii), using the same labeling scheme as Fig. 3. Here, the separation is defined as the center-to-center distance of two input pulses.

spike. Another excitation becomes possible once the system is approaching the steady state again, although while G and Q are depleted, more input energy is required to displace to $G \simeq Q+1$. As a consequence, during this relative refractory period an input which would typically generate a spike now results in a sub-threshold response.

D. Coincidence Detection

Taking advantages of the temporal integration and threshold response properties demonstrated in Sec. III-B, we stimulate the laser neuron with a pair of input pulses, which individually are below the excitation threshold, with a width of $0.4-0.5 \,\mathrm{ns}$. If they are well-separated, then there is no output pulse response, but if two input pulses are close enough a single spike is generated. This phenomenon can be exploited to perform coincidence detection, as demonstrated in Fig. 5. In inset (i), the two input pulses (blue curve) have a center-tocenter separation of 0.4 ns. This is sufficiently close to be coincident, and thus a single distinguishable output spike (red curve) is produced after the arrival of the second input pulse. This single response pulse is seen for separations of up to 0.6 ns, beyond which each input pulse yields a subthreshold oscillation. An example of this null response is shown in the inset (ii) of Fig. 5, where the temporal separation of two input pulses is 0.8 ns. Our system can thus perform coincidence detection with sub-1 ns precision. Furthermore, due to the wide optical bandwidth of a photodetector, we can perform coincidence measurements on signals of different wavelengths or from different channels.

Simulations of Eq. (1) also demonstrate coincidence detection. The same parameters as in Sec. III-B are used in Fig. 5, except for $\beta_n=12\,\mathrm{MHz}$. Note that the single response spikes following a positive coincidence detection are strongly

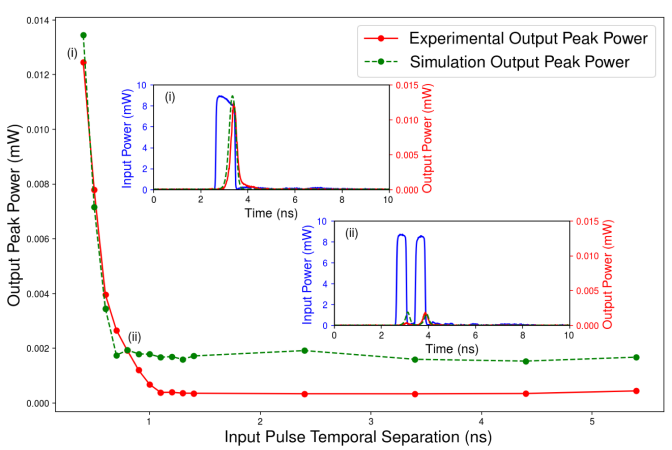


Figure 5. Response of a spiking laser neuron designed to perform coincidence detection: two pulses of varying center-to-center separation are input and the output peak power is plotted. Insets (i) and (ii) show signal traces corresponding to input pulses separated by 0.4 ns and 0.8 ns, using the same labeling scheme as Fig. 3.

in agreement with experimental results. For large pulse separations, the model predicts a significantly higher subthreshold oscillation amplitude than what was observed experimentally. This is likely a result of additional loss processes and input filtering not included in our simple Yamada model. Importantly, this model captures the dynamics of positive coincidence detection well, and for separations beyond 0.6 ns, still predicts a small subthreshold oscillation.

IV. XOR CLASSIFICATION WITH PHOTONIC SPIKING NEURAL NETWORKS

In this section, we propose a method that is compatible to our current hardware architecture to solve the XOR classification problem using spiking dynamics.

A. Method and Procedure

XOR classification can be performed by a spiking neural network with the structure shown in Fig. 6. This network consists of an input layer, a hidden layer and a readout layer. In the input layer, the input bit string is encoded into optical pulses, with different optical channels used to represent different bits. For example, if the i^{th} bit is "1", then a pulse will be generated in i^{th} channel and sent to the hidden layer. Otherwise, no pulse will be generated. Connections between input pulses (I1, I2) and the two spiking neurons (H1, H2) in the hidden layer are weighted by W_{ij} , where i represents the index of input bit, and j represents the index of hidden layer neuron. The weight configuration W_{ij} is designed with W_{11} and W_{21} larger than W_{12} and W_{22} , such that H1 will fire a spike if it receives one of the input pulses, but H2 does not fire unless two coincident pulses are received. Finally, the synaptic weight between H1 and the readout neuron (R1) is chosen to be positive, and the weight between H2 and R1 negative. With these settings, if both H1 and H2 fire, the latter is inhibitory and prevents R1 from spiking. Thus R1 only fires a spike if it receives the excitatory pulse from just H1. In summary, the

procedure of implementing an XOR operation in a photonic spiking neural network is the following:

- 1) Encode input bit information into optical spikes.
- 2) Weight input pulses in a way that $W_{11} = W_{21} > W_{12} = W_{22} > 0$, and send them to neurons in the hidden layer simultaneously.
- 3) Weight outputs of H1 and H2 and send to R1, where $W_{output1} > 0 > W_{output2}$.
- 4) The final result is "1" if R1 spikes, and "0" if otherwise. In this spiking neural network, three neurons are identical and the simulation parameters of them are the same as shown in III-B except for different bias condition A-B=0.43, and better input coupling coefficient $\theta=0.8$. All the synaptic weights are chosen by optimizing the outcome of simulation. The logic circuit analogy of this spiking neural network is shown in Fig. 6(b). In the hidden layer, H1 functions as OR gate, and H2 has the function as AND gate. This "AND" functionality is H2 performing coincidence detection. In the readout layer, the NOT operation results from the inhibitory synapse between H2 and R1.

B. Hardware Architecture

The proposed hardware architecture for the XOR operation with integrated laser neurons is shown in Fig. 6 (c). The input bit information is initially given by RF signal, and then transferred to optical pulses by modulating CW lasers with Mach-Zehnder modulator (MZM). The input optical pulse is then sent to the spiking neural network on a photonic chip. The neurons are the two-section DFB lasers presented in Section. II, and each weight connection is implemented by a semiconductor optical amplifier (SOA) and a Mach-Zehnder interferometer (MZI). SOAs provide the gain to the signal and MZIs determine the portion of light going to excitatory and inhibitory channels. The final output of R1 will be connected to a sampling scope for the readout.

C. Classification Result and Discussion

The dynamics of spiking neurons in hidden layer and readout layer are shown in Fig. 7. Here, we only show results for "01" and "11" since "10" is the same case as "01" and "00" is a trivial case where no pulse processes in the network. For the input="01", H1 and H2 receive a input from the second channel. However, since $W_{21} > W_{22}$, the input to H1 is stronger than H2. As a result H1 fires but H2 stays below threshold, as seen in Fig. 7(c-d). Moving on to the readout layer in Fig. 7(g), R1 receives an excitatory perturbation from H1, which results in a spike fired by R1 and the successful XOR operation on "01". In the case with input="11", H1 and H2 receive input pulses from both channels. The coincident input pulses to H2 provides a strong enough perturbation to generate a spike, and as shown in Figs. 7 (e-f), both H1 and H2 fire. Due to the inhibitory weight of H2's output, the total input to R1 is now below threshold. As shown in Fig. 7 (h), this prevents R2 from firing, yielding the desired final XOR readout=0.

We attribute the success of XOR classification to the

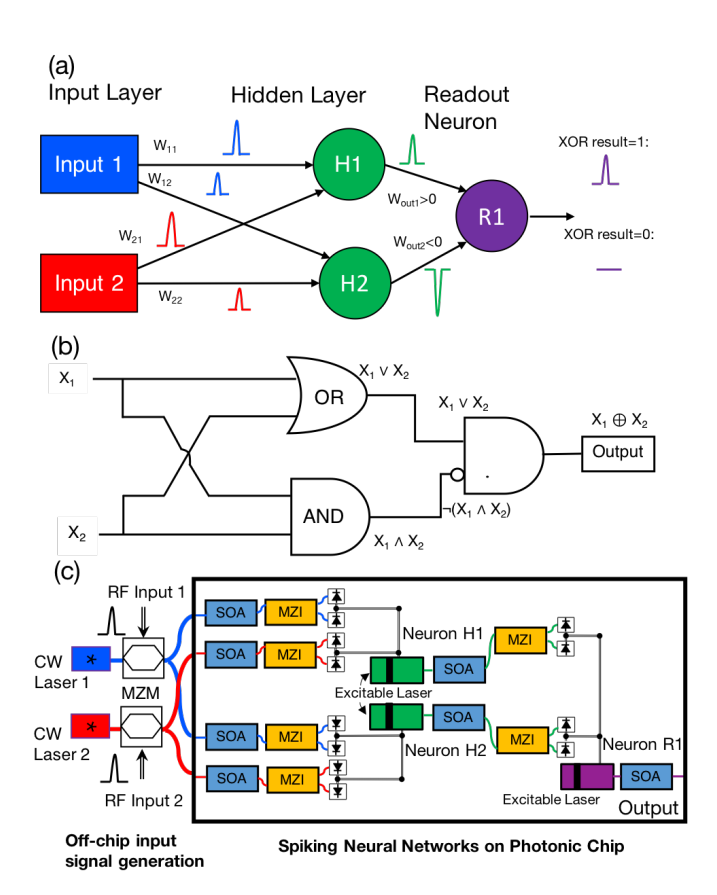


Figure 6. (a) Schematic figure of a photonic neural network that implements XOR operation. Input from 1^{st} and 2^{nd} channels are in blue and red respectively. Since the weights W_{11} , W_{12} are higher, the pulse sent to H1 has larger amplitude as shown in the figure. The outputs of H1 and H2 are in green, and the output of R1 is in purple. (b) A circuit analogy to Fig. 6. H1 acts as OR operation, H2 acts as AND operation, and R1 functions as an AND but performs a NOT operation to the input from R2 first. (c) Hardware implementation of XOR operation in a photonic spiking neural network. The input bit information is coded in RF domain and transferred to optical domain by modulation. The laser 1 in blue represents the first bit and the laser 2 in red represents the second bit. The input is then split and sent to chip. SOA, MZI, lasers, and balanced PDs are on the same III-V photonic chip. In this figure, the green excitable lasers represent neuron H1 and H2, and the purple one represents readout neuron R1.

dynamics of spiking neurons, which includes the threshold response, temporal integration, and inhibitatory dynamics. The threshold of a spiking neuron differentiates different strengths of inputs. It contributes to the desired outcomes for H1 and H2 (only H1 fires) when the input is "10" or "01", and the success of final readout in R1. When input is "11", we require H2 to fire and temporal integration plays a role here. Within a temporal integration window, the sum of two sub-threshold inputs can cause H2 to fire. Because of this temporal integration window, this network shows the tolerance of the temporal position of two input pulses. In Fig. 8, when timing jitter in the input signals is less than an input pulse width, we show that the XOR classification still performs perfectly. When the timing jitter is greater than an input pulse width, the accuracy reduces to ≈ 0.75 is because "11" case fails and leads to a truth table of OR gate. The inhibitory synapse contributes to the cancellation of H1 and H2's output, which is necessary for

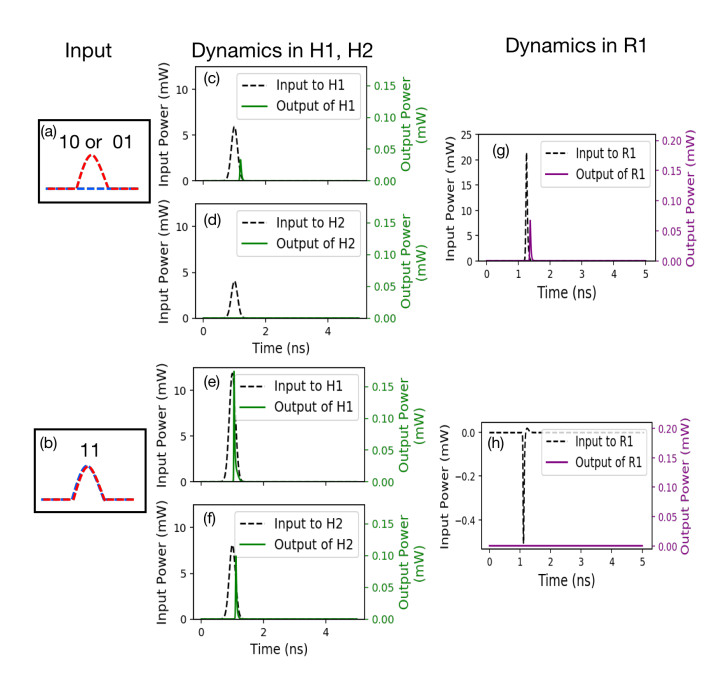


Figure 7. The two input cases "10" (equivalent to "01") and "11" are shown in (a) and (b), where blue dashed line represents the first bit and the red dashed line represents the second bit. The simulated dynamics of H1 and H2 in response are shown in (c)-(f). The black dashed line is the total input and the laser neuron output is in green. The dynamics of readout neuron R1 is shown in (g) and (h) in purple. R1 generates a spike in the "10" case, but not "11", as desired. The negative input power shown in (h) represents the photocurrent flow out of the gain section.

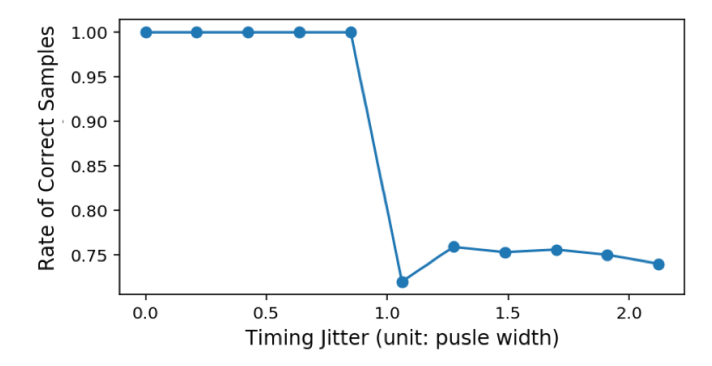


Figure 8. Simulations of the robustness of the XOR classification network to timing jitter. The accuracy is measured by inputting 1000 randomly generated two-bit binary samples under different timing jitter conditions and comparing the result to the XOR truth table. Timing jitter is the center-to-center input pulse separation, normalized to the input pulse width of 0.2355 ns.

the successful XOR operation on "11". Experimentally, the function of inhibitatory PD of this device has been tested and demonstrated in Ref. [23].

V. CONCLUSION

We constructed a photonic spiking neuron in integrated photonic circuits and experimentally studied its temporal characteristics, in particular the threshold response to integrated inputs and refractory period. The refractory period experiment indicates that the spiking laser neuron is capable of a GHz spike processing rate, and coincidence detection was

performed with ns precision. These results affirm the ability to perform high speed and precision signal processing with such devices. We simulated the laser neuron dynamics using the Yamada model, and demonstrated agreement with our experimental results. Lastly, a network of integrated laser neurons to perform XOR operation was proposed. The numerical simulation of the device shows that, when proper synaptic weights are chosen, XOR classification can be performed with three laser neurons with 100% accuracy even in the presence of timing jitter. This resilience to timing jitter in input pulses is thanks to the neuron's ability to perform temporal integration. The chip demonstrates the basic functionality of a photonic neuron, including robust excitability. Additionally, the photodetector-driving mechanism allows for the simple implementation of inhibitory synaptic weights, and more importantly is capable of processing information on different wavelengths or channels, dramatically increasing the computing efficiency of this system [23]. Although the scalability of this system needs to be further studied, this architecture with an O/E/O link in integrated photonic circuits offers the potential for high speed spiking neural networks. In conclusion, this integrated photonic neuron is a promising foundation for a scalable spike processor with dramatic improvements in information processing speed.

ACKNOWLEDGMENT

The authors would like to thank the Fraunhofer Heinrich Hertz Institute for their PIC fabrication services and custom laser design, as well as PhoeniX and JePPIX for their design and logistical support. This work is supported by National Science Foundation (NSF) Enhancing Access to the Radio Spectrum (EARS award 1642991) and Energy-Efficient Computing: from Devices to Architectures (E2CDA award 1740262) programs. Funding for B.J.S. was provided by the Natural Sciences and Engineering Research Council of Canada (NSERC).

REFERENCES

- J. Hasler and B. Marr, Frontiers in Neuroscience, vol. 7, no. 7 SEP, p. 118, 2013.
- [2] P. A. Merolla, J. V. Arthur, R. Alvarez-Icaza, A. S. Cassidy, J. Sawada, F. Akopyan, B. L. Jackson, S. K. Esser, R. Appuswamy, B. Taba, A. Amir, and M. Flickner, "Merolla communication network and interface a million spiking-neuron integrated circuit with a scalable," 2014.
- [3] T. F. de Lima, H.-T. Peng, A. N. Tait, M. A. Nahmias, H. B. Miller, B. J. Shastri, and P. R. Prucnal, "Machine learning with neuromorphic photonics," *J. Lightwave Technol.*, vol. 37, no. 5, pp. 1515–1534, Mar 2019.
- [4] P. R. Prucnal and B. J. Shastri, *Neuromorphic Photonics*. Boca Raton, FL, USA: CRC Press, Taylor & Francis Group, 2017.
- [5] M. A. Arbib, "The handbook of brain theory and neural networks," 2007.
- [6] W. Maass, "Computing with spiking neurons," W. Maass and C. M. Bishop, Eds. Cambridge, MA, USA: MIT Press, 1999, pp. 55–85.
- [7] P. Y. Ma, B. J. Shastri, T. F. de Lima, C. Huang, A. N. Tait, M. A. Nahmias, H.-T. Peng, and P. R. Prucnal, "Simultaneous excitatory and inhibitory dynamics in an excitable laser," *Opt. Lett.*, vol. 43, no. 15, pp. 3802–3805, Aug 2018.
- [8] B. Romeira, R. Avó, J. M. L. Figueiredo, S. Barland, and J. Javaloyes, in *Scientific reports*, 2016.
- [9] F. Selmi, R. Braive, G. Beaudoin, I. Sagnes, R. Kuszelewicz, and S. Barbay, *Physical Review Letters*, vol. 112, no. 18, p. 183902, 2014.
- [10] B. J. Shastri, M. A. Nahmias, A. N. Tait, A. W. Rodriguez, B. Wu, and P. R. Prucnal, *Scientific Reports*, vol. 6, 2016.

- [11] B. Benjamin, P. Gao, E. McQuinn, S. Choudhary, A. Chandrasekaran, J.-M. Bussat, R. Alvarez-Icaza, J. Arthur, P. Merolla, and K. Boahen, "Neurogrid: A mixed-analog-digital multichip system for large-scale neural simulations," *Proceedings of the IEEE*, vol. 102, no. 5, pp. 699– 716, May 2014.
- [12] F. Akopyan, J. Sawada, A. Cassidy, R. Alvarez-Icaza, J. Arthur, P. Merolla, N. Imam, Y. Nakamura, P. Datta, G.-J. Nam, B. Taba, M. Beakes, B. Brezzo, J. Kuang, R. Manohar, W. Risk, B. Jackson, and D. Modha, "Truenorth: Design and tool flow of a 65 mw 1 million neuron programmable neurosynaptic chip," *IEEE Transactions on Computer-Aided Design of Integrated Circuits and Systems*, vol. 34, no. 10, pp. 1537–1557, Oct 2015.
- [13] M. Davies, N. Srinivasa, T.-H. Lin, G. N. Chinya, Y. Cao, S. H. Choday, G. D. Dimou, P. Joshi, N. Imam, S. Jain, Y. Liao, C.-K. Lin, A. Lines, R. Liu, D. Mathaikutty, S. McCoy, A. Paul, J. Tse, G. Venkataramanan, Y.-H. Weng, A. Wild, Y. Yang, and H. Wang, "Loihi: A neuromorphic manycore processor with on-chip learning," *IEEE Micro*, vol. 38, pp. 82–99, 2018.
- [14] S. Furber, F. Galluppi, S. Temple, and L. Plana, "The spinnaker project," Proceedings of the IEEE, vol. 102, no. 5, pp. 652–665, May 2014.
- [15] H. J. Wünsche, O. Brox, M. Radziunas, and F. Henneberger, "Excitability of a semiconductor laser by a two-mode homoclinic bifurcation," *Physical Review Letters*, vol. 88, p. 023901, Dec 2001.
- [16] B. Romeira, J. Javaloyes, C. N. Ironside, J. M. L. Figueiredo, S. Balle, and O. Piro, "Excitability and optical pulse generation in semiconductor lasers driven by resonant tunneling diode photo-detectors," *Optics Express*, vol. 21, no. 18, pp. 20931–20940, Sep 2013.
- [17] L. Gelens, L. Mashal, S. Beri, W. Coomans, G. Van der Sande, J. Danckaert, and G. Verschaffelt, "Excitability in semiconductor microring lasers: Experimental and theoretical pulse characterization," *Physical Review A*, vol. 82, p. 063841, Dec 2010.
- [18] M. P. Fok, Y. Tian, D. Rosenbluth, and P. R. Prucnal, "Asynchronous spiking photonic neuron for lightwave neuromorphic signal processing," *Optics Letters*, vol. 37, no. 16, pp. 3309–3311, Aug. 2012.
- [19] A. Hurtado and J. Javaloyes, "Controllable spiking patterns in long-wavelength vertical cavity surface emitting lasers for neuromorphic photonics systems," *Applied Physics Letters*, vol. 107, no. 24, 2015.
- [20] M. A. Nahmias, B. J. Shastri, A. N. Tait, and P. R. Prucnal, *IEEE Journal of Selected Topics in Quantum Electronics*, vol. 19, no. 5, 2013.
- [21] H.-T. Peng, M. A. Nahmias, T. F. de Lima, A. N. Tait, and B. J. Shastri, IEEE Journal of Selected Topics in Quantum Electronics, vol. 24, no. 6, pp. 1–15, Nov 2018.
- [22] H.-T. Peng, M. A. Nahmias, T. F. de Lima, A. N. Tait, B. J. Shastri, and P. R. Prucnal, in 2018 IEEE Photonics Conference (IPC), Sept 2018, pp. 1–2.
- [23] M. A. Nahmias, H.-T. Peng, T. F. de Lima, C. Huang, A. N. Tait, B. J. Shastri, and P. R. Prucnal, "A teramac neuromorphic photonic processor," in 2018 IEEE Photonics Conference (IPC), Sept 2018, pp. 1–2.
- [24] A. N. Tait, T. Ferreira de Lima, M. A. Nahmias, H. B. Miller, H.-T. Peng, B. J. Shastri, and P. R. Prucnal, "Silicon photonic modulator neuron," *Phys. Rev. Applied*, vol. 11, p. 064043, Jun 2019. [Online]. Available: https://link.aps.org/doi/10.1103/PhysRevApplied.11.064043
- [25] K. Vandoorne, P. Mechet, T. Van Vaerenbergh, M. Fiers, G. Morthier, D. Verstraeten, B. Schrauwen, J. Dambre, and P. Bienstman, "Experimental demonstration of reservoir computing on a silicon photonics chip," *Nature Communications*, vol. 5, pp. 3541 EP –, 03 2014. [Online]. Available: http://dx.doi.org/10.1038/ncomms4541
- [26] P. R. Prucnal, B. J. Shastri, T. F. de Lima, M. A. Nahmias, and A. N. Tait, "Recent progress in semiconductor excitable lasers for photonic spike processing," *Adv. Opt. Photon.*, vol. 8, no. 2, pp. 228–299, Jun 2016.
- [27] E. M. Izhikevich, IEEE Transactions on Neural Networks, vol. 15, no. 5, pp. 1063–1070, 2004.
- [28] M. J. Berry and M. Meister, "Refractoriness and neural precision," The Journal of neuroscience: the official journal of the Society for Neuroscience, vol. 18 6, pp. 2200–11, 1997.
- [29] J. J. Hopfield, "Pattern recognition computation using action potential timing for stimulus representation," *Nature*, vol. 376, pp. 33–36, 1995.
- [30] R. Gütig and H. Sompolinsky, "The tempotron: a neuron that learns spike timingbased decisions," *Nature Neuroscience*, vol. 9, pp. 420–428, 2006.
- [31] F. Kamaruzaman, A. A. Shafie, and Y. Mohd-Mustafah, "Coincidence detection using spiking neurons with application to face recognition," *J. Applied Mathematics*, vol. 2015, pp. 534 198:1–534 198:20, 2015.
- [32] M. Tsukada and X. Pan, "The spatiotemporal learning rule and its efficiency in separating spatiotemporal patterns," *Biological cybernetics*, vol. 92, pp. 139–46, 03 2005.

- [33] F. Selmi, R. Braive, G. Beaudoin, I. Sagnes, R. Kuszelewicz, and S. Barbay, "Temporal summation in a neuromimetic micropillar laser," *Opt. Lett.*, vol. 40, no. 23, pp. 5690–5693, Dec 2015.
- [34] M. A. Nahmias, A. N. Tait, L. Tolias, M. P. Chang, T. Ferreira de Lima, B. J. Shastri, and P. R. Prucnal, *Applied Physics Letters*, vol. 108, no. 15, p. 151106, 2016.
- [35] JePPIX Design Libraries, 2019. [Online]. Available: http://www.jeppix. eu/pdk
- [36] M. Yamada, "A theoretical analysis of self-sustained pulsation phenomena in narrow-stripe semiconductor lasers," *IEEE Journal of Quantum Electronics*, vol. 29, no. 5, pp. 1330–1336, May 1993.
- [37] J. L. Dubbeldam, B. Krauskopf, and D. Lenstra, "Excitability and coherence resonance in lasers with saturable absorber." *Physical Review* E, vol. 60, no. 6, pp. 6580–6588, 1999.

Hsuan-Tung Peng received the B.S. degree from National Taiwan University with a B.S. in physics in 2015, and an M.A. from Princeton University in Electrical Engineering in 2018. He is now pursuing a Ph.D. degree at Princeton University, Princeton NJ, USA. His current research interests include neuromorphic photonics, photonic integrated circuits, and optical signal processing.

Gerasimos Angelatos received a B.S.E. in Engineering Physics in 2014 from Queen's University, Canada, and an M.Sc. in 2015 advised by Dr. Stephen Hughes from the same institution. He earned a M.A. and is currently completing his Ph.D. in Electrical Engineering at Princeton University as a member of Dr. Hakan Türeci's Quantum Optics Group. He is a recipient of the NSERC Postgraduate Scholarship and the Francis Robbins Upton Fellowship from Princeton. His current research interests include neuromorphic systems, quantum engineering, quantum noise, and quantum optics in complex media.

Thomas Ferreira de Lima received a bachelors degree and the Ingénieur Polytechnicien masters degree from Ecole Polytechnique, Palaiseau, France, with a focus on Physics for Optics and Nanosciences. He is working toward the Ph.D. degree in Electrical Engineering in the Lightwave Communications Group, Department of Electrical Engineering, Princeton University, Princeton, New Jersey. His research interests include integrated photonic systems, nonlinear signal processing with photonic devices, spike-timing-based processing, ultrafast cognitive computing, and dynamical lightmatter neuro-inspired learning and computing. He is also a contributing author to the textbook, *Neuromorphic Photonics*.

Mitchell A. Nahmias received a B. S. (Honors) in Electrical Engineering with a Certificate in Engineering Physics in 2012, and an M.A. in Electrical Engineering 2014, both from Princeton University. He is currently finishing his Ph.D. degree as a member of the Princeton Lightwave Communications Laboratory. He was a research intern at the MIRTHE Center in Princeton, NJ during the summers of 2011-2012 and L-3 Photonics during the summer of 2014 in Carlsbad, CA. His research interests include laser excitability, photonic integrated circuits, unconventional computing, and neuromorphic photonics. Mr. Nahmias is a Student Member of the IEEE Photonics Society and the Optical Society of America (OSA) and has authored or co-authored more than 50 journal or conference papers. He was the recipient of the Best Engineering Physics Independent Work Award (2012), the National Science Foundation Graduate Research Fellowship (NSF GRFP), the Best Paper Award at IEEE Photonics Conference 2014 (third place), and the Best Paper award at the 2015 IEEE Photonics Society Summer Topicals Meeting Series (first place). He is also a contributing author to the textbook, Neuromorphic Photonics.

Alexander N. Tait received his PhD in the Lightwave Communications Research Laboratory, Department of Electrical Engineering, Princeton University, Princeton, NJ, USA, advised by Professor Paul Prucnal. He also received the B.Sci.Eng. (Honors) at Princeton in Electrical Engineering in 2012. His research interests include silicon photonics, optical signal processing, optical networks, and neuromorphic engineering. Dr. Tait is a recipient of the National Science Foundation Graduate Research Fellowship and is a Student Member of the IEEE Photonics Society and the Optical Society of America (OSA). He is the recipient of the Award for Excellence from the Princeton School of Engineering and Applied Science (SEAS), the Optical Engineering Award of Excellence from the Princeton Department of Electrical Engineering, the Best Student Paper Award at the 2016 IEEE Summer Topicals Meeting Series, and the Class of 1883 Writing Prize from the Princeton Department of English. He has authored 9 refereed papers and a book chapter, presented research at 13 technical conferences, and contributed to the textbook Neuromorphic Photonics

Siamak Abbaslou received M.S. and Ph.D. degree in electrical engineering from Rutgers University, New Jersey in 2017 and 2015 respectively. Since 2017 he has been with the Lightwave lab, at Princeton university, where he is engaged in work on fabrication and development of electro-optic modulators on silicon. His current research interest includes fabrication, simulation and characterization of silicon photonic structures with passive and active photonic integrated circuits for optical signal processing applications.

Bhavin J. Shastri (M' 11) is an Assistant Professor of Engineering Physics at Queen's University, Canada. He is a co-author of the book, *Neuromorphic Photonics* (Taylor & Francis, CRC Press). He was an Associate Research Scholar (2016-2018) and Banting and NSERC Postdoctoral Fellow (2012-2016) at Princeton University. He received the Ph.D. degree in electrical engineering (photonics) from McGill University in 2012. Dr. Shastri is a recipient of the 2014 Banting Postdoctoral Fellowship from the Government of Canada, the 2012 D. W. Ambridge Prize for the top graduating Ph.D. student, an IEEE Photonics Society 2011 Graduate Student Fellowship, a 2011 NSERC Postdoctoral Fellowship, a 2011 SPIE Scholarship in Optics and Photonics, a 2008 NSERC Alexander Graham Bell Canada Graduate Scholarship, including the Best Student Paper Awards at the 2014 IEEE Photonics Conference, 2010 IEEE Midwest Symposium on Circuits and Systems, the 2004 IEEE Computer Society Lance Stafford Larson Outstanding Student Award, and the 2003 IEEE Canada Life Member Award.

Paul R. Prucnal (F' 92) received his A.B. In mathematics and physics from Bowdoin College, graduating summa cum laude. He then earned M.S., M.Phil. and Ph. D. degrees in electrical engineering from Columbia University. After his doctorate, Prucnal joined the faculty at Columbia University, where, as a member of the Columbia Radiation Laboratory, he performed groundbreaking work in OCDMA and self-routed photonic switching. In 1988, he joined the faculty at Princeton University. His research on optical CDMA initiated a new research field in which more than 1000 papers have since been published, exploring applications ranging from information security to communication speed and bandwidth. In 1993, he invented the "Terahertz Optical Asymmetric Demultiplexer," the first optical switch capable of processing terabit per second (Tb/s) pulse trains. Prucnal is author of the book, Neuromorphic Photonics, and editor of the book, Optical Code Division Multiple Access: Fundamentals and Applications. He was an Area Editor of IEEE Transactions on Communications. He has authored or co-authored more than 350 journal articles and book chapters and holds 28 U.S. patents. He is a fellow of the Institute of Electrical and Electronics Engineers(IEEE), the Optical Society of America (OSA) and the National Academy of Inventors (NAI), and a member of honor societies including Phi Beta Kappa and Sigma Xi. He was the recipient of the 1990 Rudolf Kingslake Medal for his paper entitled "Self-routing photonic switching with optically-processed control, received the Gold Medal from the Faculty of Mathematics, Physics and Informatics at the Comenius University, for leadership in the field of Optics 2006 and has won multiple teaching awards at Princeton, including the E-Council Lifetime Achievement Award for Excellence in Teaching, the School of Engineering and Applied Science Distinguished Teacher Award, The President's Award for Distinguished Teaching. He has been instrumental in founding the field of Neuromorphic Photonics and developing the "photonic neuron", a high speed optical computing device modeled on neural networks, as well as integrated optical circuits to improve wireless signal quality by cancelling radio interference.